J. Fluid Mech. (1995), *vol.* 301, *pp.* 345–370

The effect of rotation on double-diffusive convection in a laterally heated vertical slot

By OLIVER S. KERR

City University, Northampton Square, London EC1V 0HB, UK

(Received 9 February 1995)

The effect of rotation about a vertical axis on the linear stability of a salt-stratified fluid enclosed in a vertical slot when subjected to a temperature difference between the walls is investigated. It is found that for large salinity stratifications there are three distinct regimes of instability for different values of the rotation rate. For small rotation rates the convection cells resemble the thin, almost flat, convection cells predicted by non-rotating theory. The effect of the rotation is to marginally destabilize the fluid whilst inducing a small slope in the convection cells along the parallel walls. As the rotation rate is increased there is an abrupt change in the form of the most unstable convection cells as their aspect ratio and slope parallel to the walls both become of order one in magnitude. As the rotation rate is further increased there is a second less abrupt transition when the internal Rossby radius of deformation based on the vertical scale of the cells becomes of the same order of size as the slot width. After this point the slope of the cells increases in proportion to the rotation rate. The asymptotic nature of these three regimes is found.

The effect of rotation on double-diffusive instabilities caused by more general horizontal temperature and salinity gradients in a salt-stratified fluid is also investigated, with particular reference to the case of heating the salinity gradient from a single sidewall. This analysis is restricted to the case where the rotation rate is low.

1. Introduction

When a stably stratified body of fluid has horizontal temperature and salinity gradients present, but no horizontal density gradient, it may be unstable to infinitesimal disturbances. These instabilities were first noticed in the context of the mixing of water masses in the oceans. Stern (1967) showed that for unbounded bodies of water with uniform horizontal temperature and salinity gradients, and where the fluxes were dominated by salt fingers, the fluid was always unstable to motions that took the form of almost horizontal interleaving convection layers. This analysis was extended by Toole & Georgi (1981) with the inclusion of viscous effects. The case of fluids with uniform gradients when the fluxes are driven by other mechanisms has been looked at by McDougall (1985), who assumed that the fluxes were proportional to the salinity difference between the convective layers and independent of the layer thicknesses, and by Holyer (1983), who assumed the fluxes were driven by molecular diffusivities. In all these cases where an unbounded fluid has uniform horizontal and vertical compositional gradients the fluid is always unstable and so considerations of marginal stability are inappropriate. Instead these studies focused on the fastest growing modes of instability.

In most applications the assumption of infinite gradients is inappropriate. More typically the horizontal gradients are confined to some finite region. Instabilities driven by horizontal gradients of finite extent have been studied by numerous authors both experimentally and theoretically. These studies come in essentially three categories: where the horizontal gradients exist between two parallel walls, where the horizontal gradients exist in a finite region between two uniformly stratified bodies of fluid, and where the horizontal gradients exist near a single boundary.

The first of these categories has been studied experimentally by Thorpe, Hutt & Soulsby (1969), Chen & Sandford (1977), Paliwal & Chen (1980). This situation has been investigated theoretically by these authors and also by Hart (1971, 1973) and Thangam, Zebib & Chen (1981). These theoretical investigations considered the marginal stability of the system under the assumption that the fluxes were driven by molecular diffusivities. Both Thorpe *et al.* and Hart looked at the case where there is a strong salinity stratification. The former made assumptions concerning boundary conditions that lead to some simplification, and the latter treated these rigorously, showing that the results of Thorpe *et al.* were the leading-order asymptotic approximation. Thangam *et al.* looked at more general salinity gradients enclosed between the walls, and showed that the first mode of instability can be oscillatory for weaker stratifications. There have been some more recent studies which fit in this category where the stability and nonlinear dynamics of salt-stratified fluid in a rectangular cavity with a laterally imposed temperature difference have been investigated numerically, for example, by Tsitverblit & Kit (1993).

The second situation has been studied experimentally by Ruddick & Turner (1979), Holyer *et al.* (1987) and Ruddick (1992). It has also been studied theoretically in the context of oceans by Niino (1986) who used the salt-finger flux model of Stern (1967). Because of the assumptions made in this flux law, the model always predicts that the fluid is unstable, and so just like the infinite gradient models it is the fastest growing mode that is considered.

The last category has been studied experimentally by many people, including Thorpe *et al.* (1969), Chen, Briggs & Wirtz (1971), Chen & Skok (1974), Linden & Weber (1977), Huppert & Turner (1980), Huppert & Josberger (1980), Tanny & Tsinober (1988, 1989) and Schladow, Thomas & Koseff (1992). This single boundary problem has also been investigated theoretically by Kerr (1989, 1990) for situations where the wall heating is not too fast, and a quasi-static approximation for the evolving background gradients can be made.

The original motivation for the work of Stern was instabilities that could develop between adjacent masses of water in the ocean, and on how these could affect their mixing. In the oceanic environment the motions often have a very large horizontal length scale and evolve on a long time scale. In such cases the Earth's rotation sometimes plays an important, if not dominating, role. For this reason there have been theoretical investigations of the effect that rotation has on the above instabilities for models with infinite horizontal gradients. Such studies have been conducted for various models of the salt and heat fluxes by Posmentier & Hibbard (1982), McDougall (1985) and Kerr & Holyer (1986). In each case they found that where the most unstable mode of instability was non-oscillatory in its nature the rotation had no effect on the growth rate of the most unstable mode. The principal effect of the rotation was to cause the intrusions to develop a slope perpendicular to the direction of the horizontal gradients. Worthem, Mollo-Christensen & Ostapoff (1983) also included the effect of horizontal shear in their analysis. This shear inhibits the growth of modes of instability that have any slope perpendicular to the horizontal

gradients, and hence they found that the rotation tended to reduce the growth rate of the fastest growing instabilities. Yoshida, Nagashima & Niino (1989) looked at the fastest growing modes in a finite region of horizontal gradients between two uniformly stratified bodies of fluids. The use of the Stern law for heat and salt fluxes in the presence of salt fingers means that in this situation, just as for the non-rotating case, the fluid is always unstable. There has been a further experimental and theoretical study of the effect of rotation on double-diffusive instabilities driven by horizontal gradients by Chereskin & Linden (1986). Their experimental study looked at the case of a heated central cylinder in a rotating tank containing a stably stratified salinity gradient. Their experiments were mostly concerned with heating rates that were far from marginal; however they did notice that the presence of rotation seemed to slow down the growth rate of the instabilities and concluded that the rotation was stabilizing. In addition they conducted a stability analysis on a salinity-stratified fluid contained between two vertical parallel walls with simplified boundary conditions at the wall, and with the assumption that there was no structure to the instabilities in the horizontal direction parallel to the walls. They found that the effect of rotation was to stabilize the fluid. This result contrasts with previously mentioned analyses which concerned models with infinite horizontal gradients. These found that the rotation did not affect the growth rate of the fastest growing mode of instability, but that a slope was introduced into these interleaving layers in a direction perpendicular to the horizontal gradients. A corollary of this is that if we assumed that there was instead no structure in this direction we would exclude from consideration the fastest growing modes of instability, and hence would find that the rotation stabilized the fluid.

The effect of rotation on double-diffusive convection in a horizontal layer has also been investigated by Pearlstein (1981). In this case there were no horizontal gradients. In an infinite body of fluid with uniform vertical salinity and temperature gradients the rotation does not affect the growth rate of the fastest growing mode. However, the presence of boundaries alters this result, and Pearlstein found that rotation could either stabilize or destabilize the fluid layer, depending on the properties of the fluid.

In this paper we will look at the effect of rotation on instabilities with finite horizontal temperature and salinity gradients while allowing the instabilities to have along-wall structure, i.e. allowing variations in the horizontal direction parallel to the walls. We will look at the slot problem that was examined by Chereskin & Linden, making the same simplifying boundary conditions, but allowing for variations horizontally along the walls. We will concentrate on the case where the salinity stratification in the fluid is, in some sense, strong and where the fluxes are driven by molecular diffusivities. This will allow us to look at the onset of instability as opposed to the fastest growing modes, and will enable us to discover what effect the rotation has on these critical modes. We find that in general for relatively small rotation rates the instabilities observed are essentially perturbations of the most unstable mode that is observed in a non-rotating slot, with a vertical size given by the Chen scale (Chen *et al.* 1971). In this case the effect of rotation is to marginally destabilize the fluid. We also find that for larger rotation rates there is another branch of solutions which corresponds to a local minimum in the heating. Initially this branch is more stable than the first branch, but for higher rotation rates still this second branch of solution becomes the most unstable and the first branch of solutions ceases to exist. This second branch of solutions has a vertical scale that is of the same order of magnitude as the width of the slot, and has two sections where different asymptotic behaviour is observed. In § 6 we look briefly at the cases where there are non-uniform

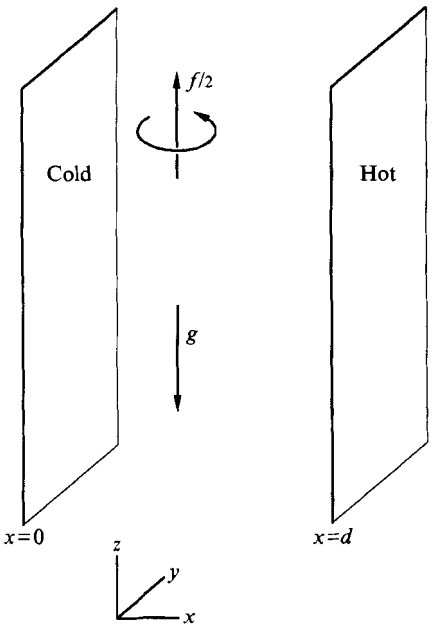

FIGURE 1. Schematic diagram showing the geometry under consideration.

horizontal gradients in either an unbounded fluid, or in a semi-infinite fluid, and when such models are valid.

2. Governing equations

We will consider the motion of a stratified fluid enclosed between two parallel vertical walls that are a distance d apart. These wall are infinite in extent and located in the planes $x = 0$ and $x = d$. The positive z-axis is taken to point in the vertical direction, and the y-axis is horizontal and parallel to the walls. The whole system is rotating with angular velocity $f/2$ about a vertical axis. We will assume that there is a horizontal temperature difference of ΔT applied across the wall with the wall at $x = d$ being the hotter. This configuration is shown schematically in figure 1. We will also assume that the temperature and salt boundary conditions are such that there is a stationary conduction solution to the governing equations. This will mean assuming that there is a fixed salinity difference applied across the slot instead of using more realistic boundary conditions such as no-flux conditions on the salinity. More realistic boundary conditions typically lead to a non-zero velocity in the basic background state which complicates the analysis. We will also be concentrating on the case of large salinity gradients, in which case these perturbations from the stationary conduction solutions examined here are confined to thin regions near the walls (see Hart 1971).

The equations for an incompressible fluid in a frame of reference rotating with angular velocity $f/2$ about the vertical axis are

$$\frac{\partial \boldsymbol{u}}{\partial t} + f\hat{\boldsymbol{z}} \wedge \boldsymbol{u} = -\frac{1}{\rho_0}\nabla p + g(\alpha T - \beta S)\hat{\boldsymbol{z}} + \nu\nabla^2 \boldsymbol{u}, \tag{2.1a}$$

$$\frac{\partial T}{\partial t} + u\overline{T}_x + w\overline{T}_z = \kappa_T \nabla^2 T, \tag{2.1b}$$

$$\frac{\partial S}{\partial t} + u\overline{S}_x + w\overline{S}_z = \kappa_S \nabla^2 S, \tag{2.1c}$$

$$\nabla \cdot \boldsymbol{u} = 0. \tag{2.1d}$$

Here $\boldsymbol{u} = (u, v, w)$ is the velocity of the fluid, p, T and S the pressure, temperature and salinity perturbations, g the acceleration due to gravity, ν the kinematic viscosity, κ_T and κ_S the heat and salt diffusivities, α the coefficient of thermal expansion and β the coefficient of density increase with respect to the addition of salt. We are assuming that the density of the fluid is given by a linear relation of the form

$$\rho = \rho_0(1 - \alpha(T - T_0) + \beta(S - S_0)), \tag{2.2}$$

where T_0 and S_0 are some reference temperature and salinity, and ρ_0 the corresponding density of the fluid. We are taking the horizontal background temperature and salinity gradients, $\overline{T}_x = \Delta T/d$ and $\overline{S}_x$ and the vertical gradients, $\overline{T}_z$ and $\overline{S}_z$ to be constant. For the unperturbed background state to be a solution to the full governing equations we will also require that the horizontal background temperature and salinity gradients have a compensating effect on the horizontal density gradient in the fluid. This gives the relationship between $\overline{T}_x$ and $\overline{S}_x$ that

$$\alpha\overline{T}_x = \beta\overline{S}_x. \tag{2.3}$$

The basic equations (2.1*a*)–(2.1*d*) are linear equations with constant coefficients, and so the solutions can be written in the form $(\boldsymbol{u}, p, T, S) = \mathrm{Re}\{(\boldsymbol{u}_0, p_0, T_0, S_0)\exp(\mathrm{i}\boldsymbol{k}\cdot\boldsymbol{x} + \lambda t)\}$, where $\boldsymbol{u}_0$, p_0, T_0 and S_0 are complex constants, λ the growth rate and $\boldsymbol{k} = (k, l, m)$ is the wavenumber vector. Substituting such a solution into the equations and eliminating $\boldsymbol{u}_0$, p_0, T_0 and S_0 leads to the characteristic equation that must be satisfied by $\boldsymbol{k}$ and λ for a non-trivial solution to exist:

$$\begin{aligned}(\lambda + \nu\mu^2)\Big\{&(\lambda + \nu\mu^2)(\lambda + \kappa_T\mu^2)(\lambda + \kappa_S\mu^2)\mu^2 + \lambda g\left(\alpha\overline{T}_z - \overline{S}_z\right)(k^2 + l^2) \\ &+ (k^2 + l^2)\mu^2 g\kappa_T\kappa_S\left(\frac{\alpha\overline{T}_z}{\kappa_T} - \frac{\beta\overline{S}_z}{\kappa_S}\right) + g\beta\overline{S}_x(\kappa_T - \kappa_S)\mu^2 km\Big\} \\ &+ f^2m^2(\lambda + \kappa_T\mu^2)(\lambda + \kappa_S\mu^2) + fg\beta\overline{S}_x(\kappa_T - \kappa_S)\mu^2 lm = 0,\end{aligned} \tag{2.4}$$

where $\mu^2 = |\boldsymbol{k}|^2 = k^2 + l^2 + m^2$.

At this point we will non-dimensionalize the variables. We will use as the important length scale the distance across the slot, d, and the corresponding time scale d^2/κ_T and velocity scale κ_T/d. We will non-dimensionalize the temperature and salinity with respect to their respective differences across the slot at any given height, i.e. temperature with respect to $\Delta T = \overline{T}_x d$ and salinity with respect to $\Delta S = \overline{S}_x d = \alpha\Delta T/\beta$. We will also at this point assume that λ is 0. This means that we are looking for marginally stable solutions where the instability does not first appear as an oscillation. For slots with weak salinity gradients Thangam *et al.* (1981) found that the initial mode of instability could be oscillatory; however we are concerned with the case of stronger stratification where they found that the initial mode of instability had real growth rate. Kerr & Holyer (1986) found that in the case of interleaving in an unbounded fluid with constant horizontal and linear gradients the most unstable mode had a growth rate that was nearly always real. The only cases where the growth rate of the most unstable modes were complex corresponded to cases where the vertical gradients had a significant destabilizing vertical temperature gradient that was comparable in its effect on the density profile to the stabilizing vertical salinity gradient. These are

not the cases that concern us here. With these scalings, and setting $\lambda = 0$, (2.4) becomes

$$\sigma\mu'^2\{\sigma\tau\mu'^8 + (k'^2 + l'^2)\mu'^2\sigma R + k'm'\mu'^2\sigma(1-\tau)H\} + f'^2\tau m'^2\mu'^4 + f\sigma(1-\tau)H\mu'^2 l'm' = 0 \tag{2.5}$$

where the primes indicate variables that are now dimensionless. Here we have introduced the dimensionless parameters $\sigma = \nu/\kappa_T$, the Prandtl number, $\tau = \kappa_S/\kappa_T$, the salt/heat diffusivity ratio, $R = g(\tau\alpha\overline{T}_z - \beta\overline{S}_z)d^4/(\nu\kappa_T)$ a vertical Rayleigh number, and $H = g\alpha\Delta T d^3/(\nu\kappa_T)$ a horizontal Rayleigh number. Note that although the definition of R allows for a vertical temperature gradient we will henceforth ignore this term and consider the vertical stratification to be due solely to a salinity gradient, but remembering that the effect of a vertical temperature gradient can be incorporated into the analysis and results in a straightforward way. This simplification is only possible when $\lambda = 0$, and so is not appropriate for the case where instabilities are either oscillatory or are growing. The assumption that R is only due to a salinity gradient is in order to simplify discussion, and to emphasize that we are concerned with situations where the initial mode of instability is non-oscillatory. Henceforth we will drop the primes from the dimensionless variables.

We have not mentioned the boundary conditions to be used. Instead of using the full physical boundary conditions where the velocity vanishes at the boundary, as do the temperature and salinity perturbations, we will use a simplified boundary condition that will make the mathematical problem more tractable, and at the same time allow the essential physics of the problem to remain. This will allow us to get an insight into the mechanisms involved in the full problem. In so doing we are essentially following the philosophy behind the adoption of, say, stress-free boundary conditions in the study of thermal convection between parallel plates. We will impose the same restriction on the solutions, i.e. that there is no fluid flux through the vertical walls at $x = 0$ and $x = 1$. In order to be able to satisfy this condition for all y and z we must, for given l and m, be able to find two real solutions to (2.5). This gives us the condition that there must be two roots, k_- and k_+, that satisfy the condition

$$k_+ - k_- = 2\pi. \tag{2.6}$$

This boundary condition has been shown to be the appropriate one to use in the case where there is no rotation and the stratification is strong (Thorpe *et al.* 1969; Hart 1971).

3. Onset of instability

As we are interested in the onset of linear instabilities, we can express the problem as finding, for a given stratification R, the minimum value of H for which non-trivial solutions to (2.1*a*)–(2.1*d*) exist that satisfy the boundary conditions. This is done by finding, for given values of l and m, the value of H for which the maximum and minimum real roots of (2.5), when considered as a polynomial in k, differ by 2π. We then minimize H as a function of l and m in order to find the critical values of the heating rate for a given stratification, R, and rotation rate, f. These calculations were performed numerically using NAG library routines, and used values of $\sigma = 7$ and $\tau = 1/80$ for the Prandtl number and the salt/heat diffusivity ratio. Typical results are shown in figures 2–4. The first of these, figure 2, shows the

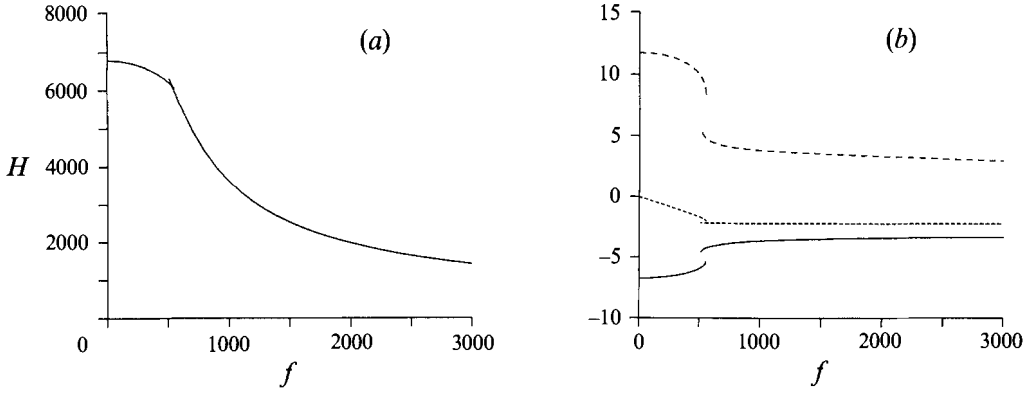

FIGURE 2. Graphs of (*a*) minimum values of H as a function of f for $R = 10^4$ and (*b*) the corresponding values of k_- (———), l (– – – –), and m (— — —).

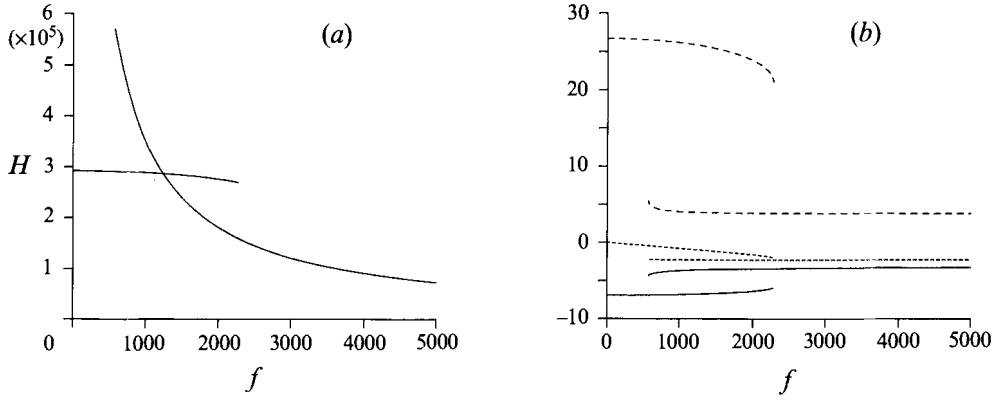

FIGURE 3. Graphs of (*a*) minimum values of H as a function of f for $R = 10^6$ and (*b*) the corresponding values of k_- (———), l (– – – –), and m (— — —).

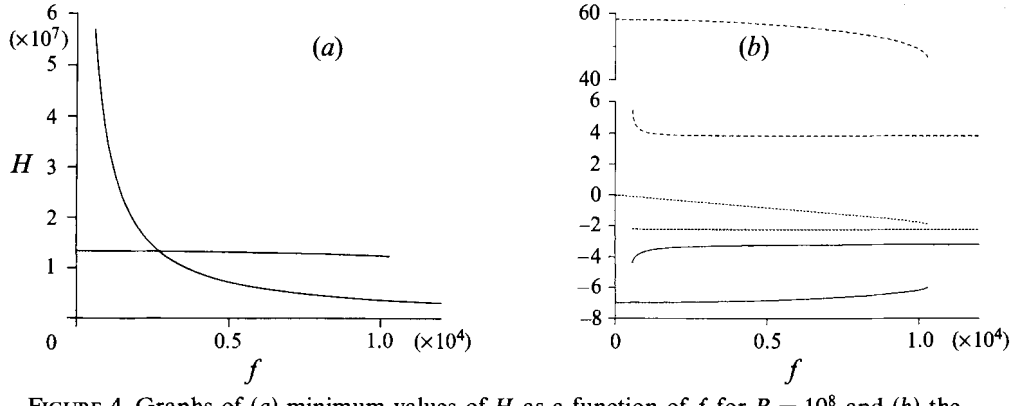

FIGURE 4. Graphs of (*a*) minimum values of H as a function of f for $R = 10^8$ and (*b*) the corresponding values of k_- (———), l (– – – –), and m (— — —).

results for $R = 10^4$. In figure 2(*a*) are shown the values of H as a function of f that have local minima in H with respect to variations in l and m. In this case there are two branches of solutions that have a small region of overlap for values of f in the region of 515.3–555.1. Up to the point of crossing the first branch represents a global minimum, and after the crossing the second branch is a global

minimum. This shows that the effect of rotation is to destabilize the fluid. On the initial branch of solutions this destabilization is not great, corresponding to a maximum decrease in the critical value of H of the order of 11% over the whole branch. Above a value of $f = 555.1$ this branch of solutions abruptly vanishes. The second branch of solutions shows a stronger decline in H as f increases. How this continues to decrease will be discussed in further detail later in this section. The corresponding values of the horizontal and vertical wavenumbers, l and m, and the value of k_- are shown in figure 2(b). Initially as f increases, the value of l steadily decreases from 0 in an approximately linear fashion, indicating the gradual tilting of the convection cells. The sense of the tilt is shown in figure 6(a). The value of m also declines as f increases, indicating a gradual increase in the vertical separation of the convection cells. The corresponding value of k_- also gradually increases. If we look at, say, the velocity component across the slot, u, we see that with our boundary conditions this velocity is zero along lines with slope $-(k_- + \pi)/m$. Initially the value of k_- is -6.739 indicating that the convection cells slope up towards the hot wall. As the rotation rate increases this slope decreases steadily, but always remains positive. On the second branch of solutions the value of l stays almost constant at around -2.2. The value of m drops abruptly by a factor of almost a half from the value on the initial branch, indicating a sudden increase in the preferred vertical length scale. The value of k_- also jumps on changing from the initial to the second branch of solutions. Subsequently it gradually increases, but never reaches $-\pi$, and so the slope of the convection cells always remains positive.

These trends are repeated in the other two sets of graphs for $R = 10^6$ and $R = 10^8$ (figures 3 and 4). However as R increases so the region of overlap between the two branches increases. In all three cases the curves of minimum H cross over as would be expected. A notable point about the variations in l and m is that in all three cases l settles down to approximately the same value on the second branch of solutions, and also the values taken by m are similar. On the first branch the value of l taken at the termination of the branch is always close to the value of l on the second branch; however the jump in the corresponding values of m increases as R increases.

If these results are plotted with logarithmic axes (figure 5) further trends become apparent. In figure 5(a) it can be seen that as R increases, the value of H varies little along the first branch. On the second branch the value decreases. The gradient in this initial section is approximately -1, indicating that H is approximately proportional to f^{-1}. This branch then goes through a further transition where H ceases to decrease and becomes almost constant. This secondary transition in the second branch of solutions is also apparent in the other graphs in figure 5(b,c). The curves of m display a region where it is approximately constant, before undergoing a transition to a regime where it decays as f^{-1}. In all cases l is almost constant on this second branch, with the curves indistinguishable on this plot as they lie on top of each other. It is also clear from these graphs that the minimum value of f for the second branches of solutions is almost identical for all three values of R.

It is apparent from the above results that there are essentially three regimes that occur for large values of R. The first corresponding to the initial branch of solutions is characterized by slowly varying values of H and m, and an l that decreases in proportion to f. We will refer to this as the small-f regime. The second regime has a steadily decreasing H, being proportional to f^{-1}, and almost constant l and m. We will refer to this as the intermediate-f regime. Lastly we have a regime

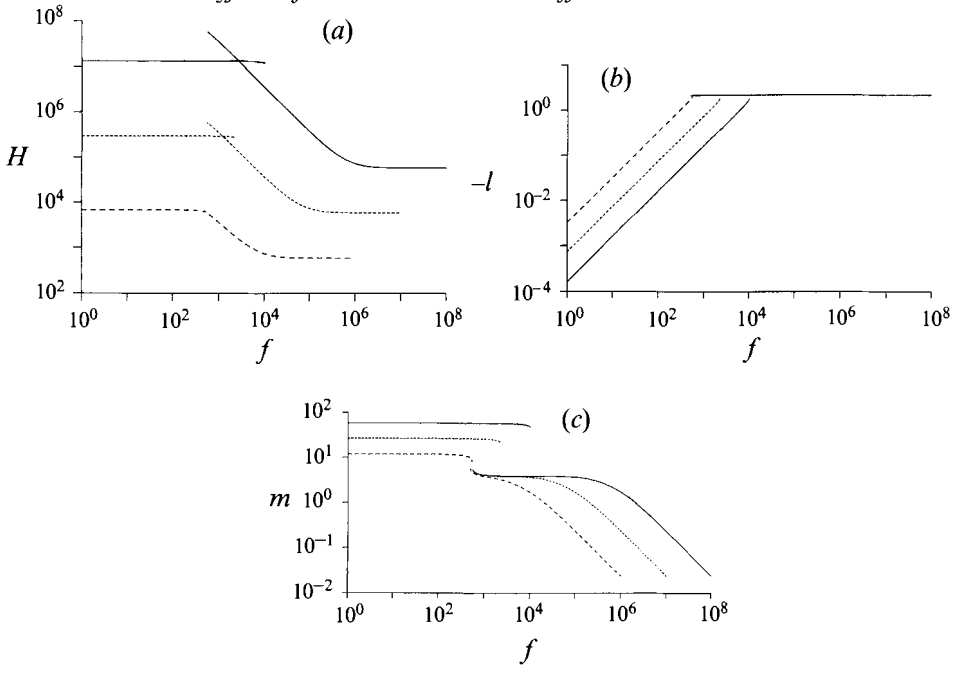

FIGURE 5. Graphs of (*a*) the minimum values of H as a function of f for $R = 10^4$ (— — —), 10^6 (– – – – –) and 10^8 (————) and the corresponding values of (*b*) $-l$ and (c) m on logarithmic axes.

where H and l are approximately constant, but m decreases as f^{-1}. We shall refer to this as the large-f regime. Representations of convection cells in each of these regimes are shown in figure 6. These are all for $R = 10^6$. The first, figure 6(*a*), shows examples of convection cells when the small-f solutions are the most unstable. Here the convection cells take the form of thin almost horizontal layers which rise slightly in the positive x-direction and in the positive y-direction. This is the same sense of slope as found by Kerr & Holyer (1986) for interleaving instabilities in an unbounded fluid with linear gradients. The second representation, figure 6(*b*), shows the most marginally stable rolls for $f = 5000$. This is in the intermediate regime. Here the convection cells are no longer flat, but form almost round cylinders with an $O(1)$ slope in the same direction as before. Lastly, figure 6(*c*) shows convection cells in the large-f regime. Now the convection cells form almost vertical cylinders. Superimposed on each of these are some streamlines of individual fluid elements. In the small-f case the convection motion is almost confined to a vertical plane that is oblique to the slot. In the intermediate-f regime the fluid element is confined to a plane that slopes slightly down from the hot wall to the cool wall. Lastly, the large-f case, the motion of a fluid element is confined almost entirely to a horizontal plane with very small slope.

The various transitions that have been observed here will be examined in more detail in the next section where the asymptotic behaviour of all three regimes will be examined. The physical interpretation of some of these results will also be given in §4 and the subsequent section.

4. Asymptotics in the strong stratification limit

The numerical solutions in the previous section show how, as R increases, the structure of the solutions becomes more clearly defined with three distinct regions of

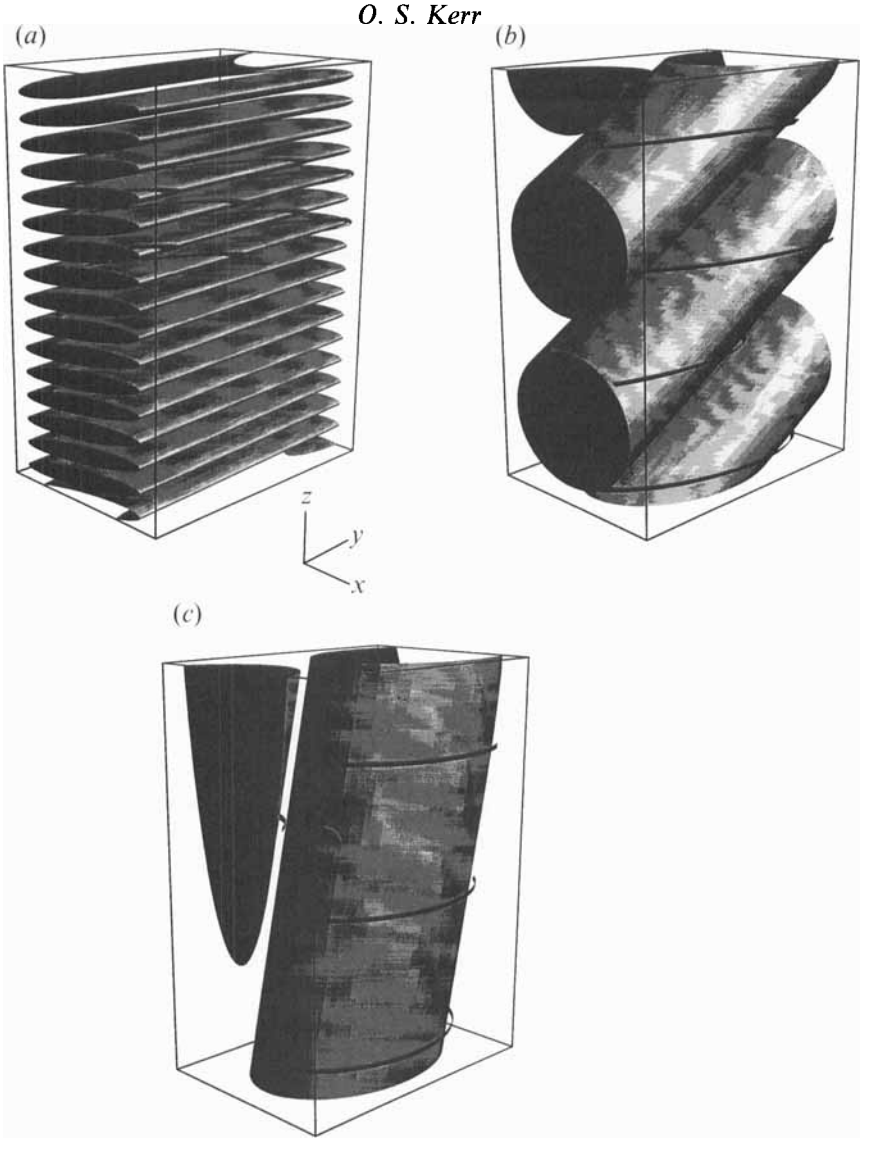

FIGURE 6. Representation of the marginally stable convection cells for $R = 10^6$ in a cell of length $2^{1/2}$ in the y-direction and 2 in the z-direction. These show cells on (*a*) the small-f branch of solutions, with $f = 1200$, (*b*) the intermediate-f branch of solutions, with $f = 5000$, and (*c*) the large-f branch of solutions, with $f = 500\,000$. Paths of fluid elements are also shown.

behaviour as f varies: the small-, intermediate- and large-f branches of solutions. In the following subsections we will look at each of these three regions of behaviour separately.

4.1. *Small-f branch*

In the case of strong stratification, $R \gg 1$, the observed instabilities, both experimentally and theoretically, for the non-rotating case consist of almost horizontal thin convection cells (Thorpe *et al.* 1969; Hart 1971). One can then make the assumption that $m \gg k, l$, and so vertical diffusion is more important than horizontal diffusion. If we assume as a result that we can ignore the horizontal derivative in the diffusion

terms (i.e. $\nabla^2 \approx \partial^2/\partial z^2$) we can re-write (2.5) as

$$\sigma m^2 \{\sigma\tau m^8 + (k^2 + l^2)m^2\sigma R + km^3\sigma(1-\tau)H\} + f^2\tau m^6 + f\sigma(1-\tau)Hm^3 l = 0. \quad (4.1)$$

With this approximation the characteristic equation is now only a quadratic in k. Before we progress further, some simplification in the algebra results if we rescale the variables to match those used by Kerr (1989) in the analysis of instabilities in a strong salinity gradient under the influence of heating at a single sidewall. The scalings used there make use of the vertical length scale

$$h = \frac{(1-\tau)\alpha\Delta T}{-\beta\bar{S}_z} = (1-\tau)H/R. \quad (4.2)$$

This is the Chen scale (Chen *et al.* 1971) with an additional factor of $(1-\tau)$. The appropriate time scale for the problem is now the diffusion time across this length scale and not over the width of the slot. With these new time and vertical length scales the rotation rate and the vertical wavenumber, m, are rescaled to give

$$\tilde{f} = fh^2/d^2 = f(1-\tau)^2H^2/R^2, \quad (4.3a)$$

and

$$\tilde{m} = mh/d = m(1-\tau)H/R. \quad (4.3b)$$

With these rescalings the strength of the lateral heating with respect to the vertical stratification can be described with a single non-dimensional number, Q, defined by

$$Q = \frac{(1-\tau)^6 g(\alpha\Delta T)^6}{\nu\kappa_S d^2\left(-\beta\bar{S}_z\right)^5} = \frac{(1-\tau)^6 H^6}{\tau R^5}. \quad (4.4)$$

The physical basis for this parameter is described in Kerr (1989).

Using the above rescalings (4.1) becomes

$$k^2 + l^2 + \tilde{m}k + \frac{\tilde{f}l}{\sigma\tilde{m}} + \frac{\tilde{m}^6}{Q} + \frac{\tilde{f}^2\tilde{m}^2}{\sigma^2 Q} = 0. \quad (4.5)$$

We can solve this quadratic in k, and so the condition (2.6) that the roots differ by 2π can be evaluated explicitly to give a relationship between Q, $\tilde{f}$, l and $\tilde{m}$:

$$\pi^2 = \tilde{m}^2/4 - l^2 - \frac{\tilde{f}l}{\sigma\tilde{m}} - \frac{\tilde{m}^6}{Q} - \frac{\tilde{f}^2\tilde{m}^2}{\sigma^2 Q}, \quad (4.6)$$

or

$$Q = \frac{\tilde{m}^2(\tilde{m}^4 + \tilde{f}^2/\sigma^2)}{\tilde{m}^2/4 - (\pi^2 + l^2 + \tilde{f}l/(\sigma\tilde{m}))}. \quad (4.7)$$

For marginal stability we want to minimize Q with respect to variations in l and $\tilde{m}$. Differentiating (4.6) with respect to l and $\tilde{m}$ gives the further pair of equations to be satisfied at the minimum:

$$0 = -2l - \frac{\tilde{f}}{\sigma\tilde{m}}, \quad (4.8)$$

$$0 = \frac{\tilde{m}}{2} + \frac{\tilde{f}l}{\sigma\tilde{m}^2} - \frac{6\tilde{m}^5}{Q} - \frac{2\tilde{f}^2\tilde{m}}{\sigma^2 Q}. \quad (4.9)$$

We can use (4.8) to eliminate l from both (4.6) and (4.9) and hence obtain a pair of

equations for Q in terms of $\tilde{m}$:

$$Q = \frac{4\tilde{m}^4\left(\tilde{m}^4 + (\tilde{f}/\sigma)^2\right)}{\tilde{m}^4 + \tilde{f}^2/\sigma^2 - 4\pi^2\tilde{m}^2} = \frac{4\tilde{m}^4\left(3\tilde{m}^4 + (\tilde{f}/\sigma)^2\right)}{\tilde{m}^4 - (\tilde{f}/\sigma)^2}. \tag{4.10}$$

These can be rearranged to obtain a quadratic in $\tilde{f}^2/\sigma^2$ in terms of $\tilde{m}$ which has the solution

$$\tilde{f}^2/\sigma^2 = \tilde{m}^2(\pi^2 - \tilde{m}^2) \pm \tilde{m}^2(4\pi^2\tilde{m}^2 + \pi^4)^{1/2}. \tag{4.11}$$

The requirement that $\tilde{f}^2 \geqslant 0$ tells us that we must take the positive root and additionally that $0 \leqslant \tilde{m}^2 \leqslant 6\pi^2$. We can also see that $\tilde{f}^2$ must have a maximum for some $\tilde{m}$ between 0 and $6^{1/2}\pi$; this occurs when

$$\tilde{m}^2 = \left(\tfrac{3}{2} + 3^{1/2}\right)\pi^2 \approx 5.648^2, \tag{4.12}$$

with corresponding values of the other parameters given by

$$\tilde{f}^2/\sigma^2 = \tfrac{3}{2}\left(\tfrac{3}{2} + 3^{1/2}\right)\pi^4 \approx 21.73^2, \tag{4.13a}$$

$$Q = 3\left(45 + 26 \times 3^{1/2}\right)\pi^4 \approx 26\,310, \tag{4.13b}$$

$$l = -\pi/2^{1/2} \approx -2.221. \tag{4.13c}$$

There are no solutions that correspond to values of $\tilde{f}$ greater than (4.13a) and so this gives the maximum rotation rate for solutions to exist on this branch of solutions. The ratio between the above value of Q and the critical value for a non-rotating slot, $432\pi^4$, is $(45 + 26 \times 3^{1/2})/144 \approx 0.6252$. This corresponds to a ratio of temperature differences of 0.9247. So, although the rotation enhances the instability, the amount by which the critical temperature difference is depressed is less than 8% for all rotation rates which are less that the critical rate given by (4.13a).

The critical value of f corresponding to (4.13a) and the associated values of m and H are

$$f = \left(\frac{3}{2}\left(\frac{3}{2} + 3^{1/2}\right)\right)^{1/2}\frac{\sigma R^2\pi^2}{(1-\tau)^2H^2}, \tag{4.14a}$$

$$m = \left(\frac{3}{2} + 3^{1/2}\right)^{1/2}\frac{\pi R}{(1-\tau)H}, \tag{4.14b}$$

$$H = \left(\frac{3\left(45 + 26 \times 3^{1/2}\right)\pi^4\tau R^5}{(1-\tau)^6}\right)^{1/6}. \tag{4.14c}$$

There are no solutions for values of $\tilde{f}$ larger than the critical value that also satisfy the condition that the value of Q is a minimum with respect to variations in l and $\tilde{m}$. For values of $\tilde{f}$ less than this maximum figure, we have found in (4.11) two values of $\tilde{m}$ where Q is stationary. The larger of the two corresponds to the minimum of Q that we require, the smaller value of $\tilde{m}$ corresponds to a saddle point. It would perhaps make the situation clearer if we again consider Q as a function of l and $\tilde{m}$. The first thing to note is that the denominator of (4.7) is zero along the lines given by

$$\tilde{m}^2/4 - (\pi^2 + l^2 + \tilde{f}l/(\sigma\tilde{m})) = 0. \tag{4.15}$$

These lines of singular Q also divide the $(l, \tilde{m})$-plane into regions where Q is either positive or negative. Negative values of Q do not correspond to situations which are physically meaningful. Q also changes sign across the line $\tilde{m} = 0$, where $Q = 0$.

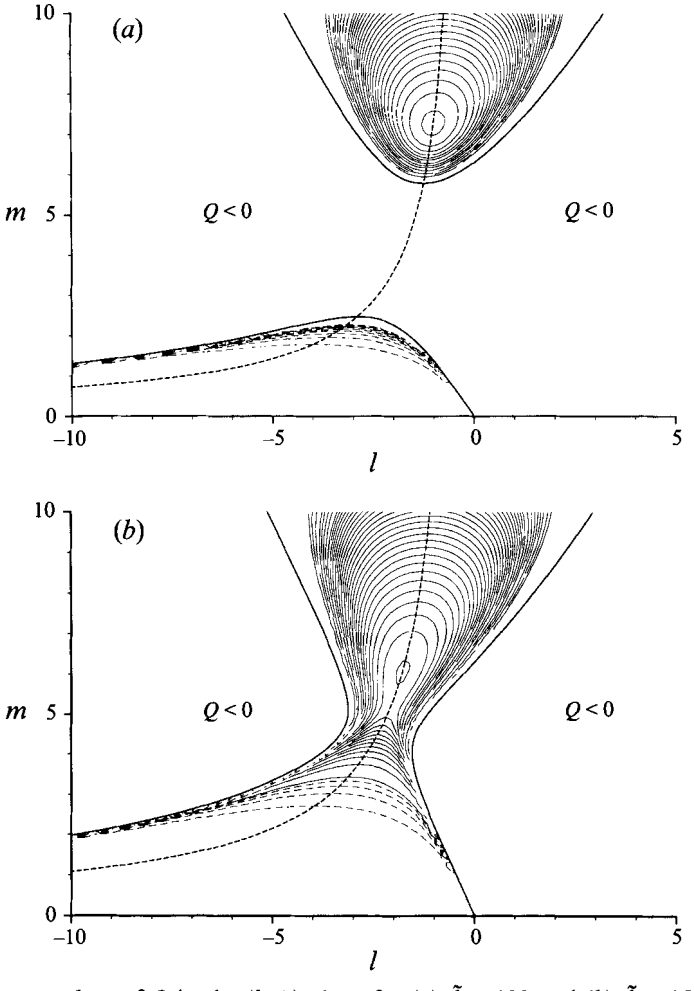

FIGURE 7. Contour plots of Q in the $(l, \tilde{m})$-plane for (*a*) $\tilde{f} = 100$ and (*b*) $\tilde{f} = 150$. In both cases Q is singular along the heavy lines, and zero along the l-axis. The continuous contours are in steps of 2500 and the dashed contours have separations of (*a*) 100 and (*b*) 500.

There are two possible regimes depending on the magnitude of $\tilde{f}$, which are shown in figure 7. In the first of these, figure 7(*a*), for lower values of $\tilde{f}$ there are two separate regions of positive Q for $\tilde{m} > 0$, while for larger values of $\tilde{f}$ the two regions join, and instead there are two regions with negative Q. In the first case Q has a local minimum in the region to the top of the figure where Q is positive. The second stationary point is a saddle point located in the central region where Q is negative. The second region of positive Q located adjacent to the negative l-axis has no stationary points: the values of Q increase monotonically from 0 along the l-axis, becoming infinite as the singular line is approached. This region will be discussed further in the next subsections. Here, we should just note that the approximations made in this subsection break down in this region.

For larger values of $\tilde{f}$ the two regions of positive Q join, and the second stationary point now lies in the region of positive Q. It is still a saddle point, separating what is now a local minimum in the positive region from the global minimum along the l-axis. When the critical value of $\tilde{f}$ is reached this local minimum and the saddle

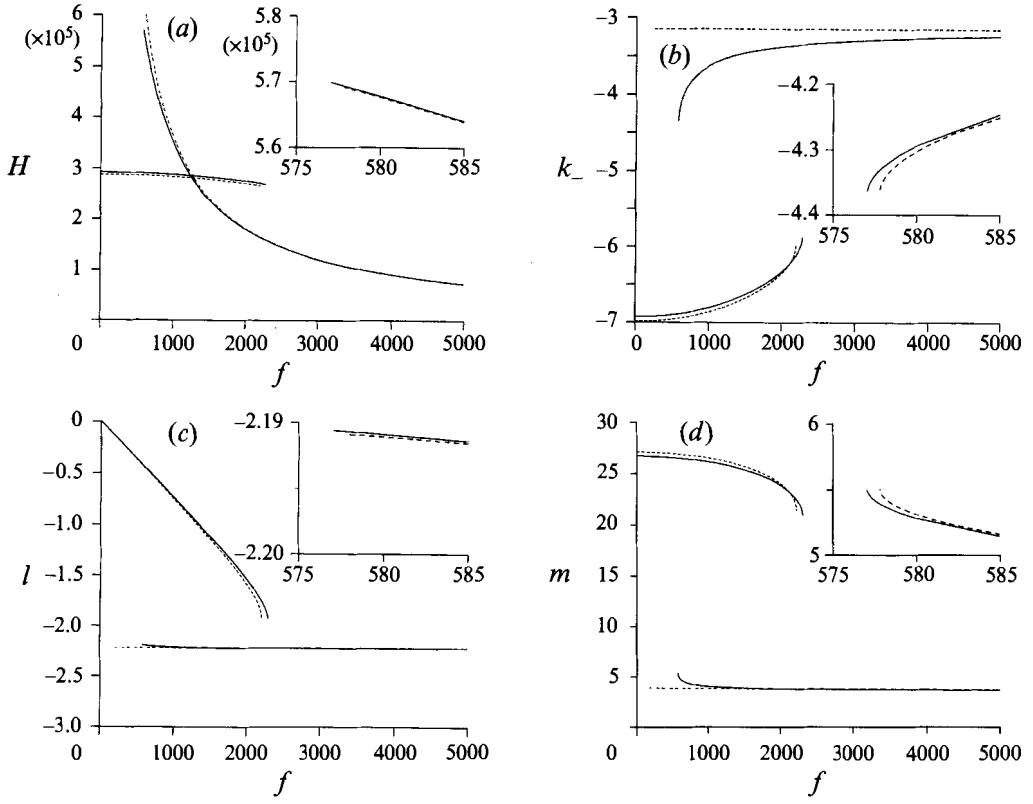

FIGURE 8. Graphs of (*a*) H, (*b*) k_-, (*c*) l and (*d*) m for f between 0 and 5000 for $R = 10^6$. The solid lines show the full solutions, while the dashed lines indicate the various asymptotic solutions: the small-f solutions (- - - - -), the basic intermediate-f solutions (-- --) and the improved intermediate-f solutions (— — —). The last of these hardly visible on the large-scale plots as they almost exactly coincide with the full solutions. They are visible in the inserts which show the termination of these solutions for f near 577.

point combine, leading to a situation where there are no stationary points, and the region of positive Q slopes down towards the l-axis where the approximations made in this subsection are not valid.

The crossover between the two regimes of figure 7 occurs when $\tilde{f} = 2\sigma\pi^2$, at which point (4.15) factorizes to $(\tilde{m} + 2l)(\tilde{m}^2 - 2l\tilde{m} - 4\pi^2)/(4\tilde{m}) = 0$.

The correspondence between this asymptotic solution and the numerical results calculated previously are shown in figure 8. This shows good agreement, which improves for larger values of R.

4.2. *Large-f branch*

The second clearly defined limit occurs when f is large. In this case an examination of (2.5) shows that the primary balances that occur as $f \to \infty$ require that $H = O(1)$, $l = O(1)$, and $m = O(f^{-1})$. The requirement that there are two roots for k that differ by 2π means that $k = O(1)$ also. This differs from the large rotation rate limit for interleaving in an infinite fluid where $k = O(f^{-1})$. With these balances the leading-order approximation to (2.5) is

$$\sigma(k^2 + l^2)\{\sigma\tau(k^2 + l^2)^4 + \sigma(k^2 + l^2)^2 R\} + f^2\tau m^2(k^2 + l^2)^2 + f\sigma(1 - \tau)Hml(k^2 + l^2) = 0. \tag{4.16}$$

Note that only even powers of k appear in this equation and thus real roots will occur in pairs differing in sign but not magnitude. The requirement that roots differ by 2π tells us that here the roots we require are $\pm\pi$. Incorporating this into the above, and defining $\hat{m} = fm$, we find

$$\sigma^2\tau(\pi^2 + l^2)^4 + \sigma(\pi^2 + l^2)^2 R + \tau\hat{m}^2(\pi^2 + l^2) + \sigma(1-\tau)H\hat{m}l = 0. \tag{4.17}$$

Since we have the constraints that for marginal stability $\partial H/\partial l = 0$ and $\partial H/\partial\hat{m} = 0$ we have the additional pair of equations

$$8\sigma^2\tau l(\pi^2 + l^2)^3 + 4l(\pi^2 + l^2)\sigma^2 R + 2l\hat{m}^2\tau + \sigma(1-\tau)H\hat{m} = 0, \tag{4.18}$$

and

$$2\hat{m}\tau(\pi^2 + l^2) + \sigma(1-\tau)Hl = 0. \tag{4.19}$$

We have not as yet used the assumption that R is large. If we do so we find that the primary balance as $R \to \infty$ is between R and $\hat{m}$, and the the effect of the $\sigma^2\tau(\pi^2 + l^2)^4$ term in (4.17) and the corresponding terms in (4.18) and (4.19) can be neglected. If this is done the resulting equations can be put in matrix form:

$$\begin{pmatrix} \pi^2 + l^2 & \pi^2 + l^2 & l \\ 2(\pi^2 + l^2) & 0 & l \\ 2l & 4l & 1 \end{pmatrix} \begin{pmatrix} \tau\hat{m}^2 \\ \sigma^2 R(\pi^2 + l^2) \\ \sigma(1-\tau)H\hat{m} \end{pmatrix} = 0. \tag{4.20}$$

For non-trivial solutions to exist for this equation the determinant of the matrix must be 0. This gives the requirement that

$$l^2 = \pi^2/2. \tag{4.21}$$

If we require $\hat{m}$ to be positive then we must take the negative root. The vector in (4.20) will be a corresponding eigenvector of the matrix, and so the elements of the vector are in the ratio

$$1 : 1 : 3\pi 2^{1/2}, \tag{4.22}$$

giving

$$l = -\pi/2^{1/2}, \tag{4.23a}$$

$$\hat{m} = fm = \sigma\pi\left(\frac{3R}{2\tau}\right)^{1/2} \tag{4.23b}$$

and

$$H = \frac{9\pi^2}{(1-\tau)}\left(\frac{\tau R}{3}\right)^{1/2}. \tag{4.23c}$$

The lines corresponding to the asymptotic values of m and H for $R = 10^6$ are shown in figure 8, showing good agreement with the previous calculated values for large f.

4.3. *Intermediate-f branch*

One of the terms of (2.5) involved in the large-f asymptotic behaviour of the previous subsection was that involving f^2. Since the terms in the coefficient of f^2 are all at most $O(1)$ quantities, this leaves us with the problem that for this term to be important f itself must also be large when R is large.

Looking at the logarithmic plots of figure 5 we see that there is a region on the second branch of solutions where the curves are approximately linear, but before the large-f asymptotic behaviour described above sets in. In this region it is clear

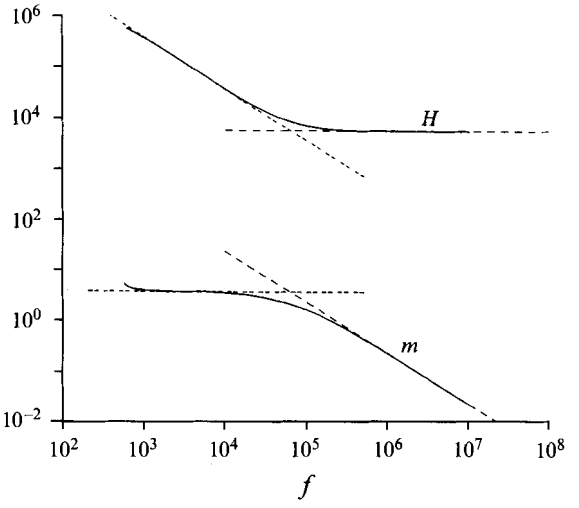

FIGURE 9. The large-f (— — —) and basic intermediate-f (-- --) asymptotic values of H and m as functions of f superimposed on the full solutions for $R = 10^6$. These show the transition between the two regimes and this branch of solutions. There is no corresponding transition in k_- or l as they remain approximately constant though both regimes.

that l and m are approximately constant, while H decreases as f^{-1}. If we arbitrarily neglect the quadratic f^2 term in (2.5) and look at the primary balances for large f we see that indeed the leading-order behaviour required is $l = O(1)$, $m = O(1)$ and $H = O(f^{-1})$. Again the boundary conditions require that $k = O(1)$. Just as in the large-f asymptotics we can assume, for large R, that the term not involving either Rayleigh number or f can be neglected. This leaves

$$\sigma(k^2 + l^2)\mu^2 R + f(1-\tau)Hml = 0. \tag{4.24}$$

Again, this only has even powers of k, and so the condition that $k_+ - k_- = 2\pi$ again gives $k^2 = \pi^2$. Finding the minimum value of H with respect to variations in l and m gives the basic intermediate-f asymptotic results that

$$l = -\pi/2^{-1/2}, \tag{4.25a}$$

$$m = (3/2)^{1/2}\pi, \tag{4.25b}$$

and

$$H = \frac{3^{3/2}\pi^2\sigma R}{(1-\tau)f}. \tag{4.25c}$$

Comparing the above results with the large-f asymptotics we can find where the transition between the two regimes occurs. If we find the value of f at which the predicted values of m and H in the two regimes are equal we find that it occurs when $f = \sigma(R/\tau)^{1/2}$ for both cases. Hence the transition occurs when, in dimensional terms, the rotation rate is a factor of $(\sigma/\tau)^{1/2}$ greater than the buoyancy frequency. This transition, and the agreement with the asymptotic theory, are shown in figure 9.

The plots of the critical values of H shown in figure 5 all show that this intermediate branch of solutions terminates for values of f just below 580, and that as f reduces towards this value the values of k_- diverge from $-\pi$. The above analysis does not reproduce this feature. However, with H growing as f^{-1} as f gets smaller we can see that the term in (2.5) involving H that we have neglected in both

the large- and the intermediate-f asymptotics will become more important. If we include this term in the intermediate-f analysis for large R then instead of (4.24) we have

$$\sigma(k^2+l^2)\mu^2 R + \sigma k m \mu^2 (1-\tau)H + f(1-\tau)Hml = 0. \tag{4.26}$$

Note that now an odd power of k has been introduced, and so we no longer have the simplification that $k_\pm = \pm\pi$. It should also be noted that if (4.26) is divided by σR then the physical parameters only appear here in the combinations f/σ and $(1-\tau)H/R$, and so the results obtained by minimizing H once for a given f/σ can be applied to other values of the parameters with suitable rescaling. The optimum value of H was found numerically subject to the constraint (4.26) and that the two roots k_+ and k_- differed by 2π. The results are shown in figure 8 with the full results for $R = 10^6$ superimposed. It is clear that there is good agreement between the results from the full characteristic equation (2.5) and the asymptotic values. With the extra term the asymptotic solutions cease to exist at a critical value of f which was found to be

$$f \approx 82.55\sigma. \tag{4.27}$$

This agrees with the results found for the full system with $\sigma = 7$ and $R = 10^8$, say, where the intermediate branch was found to exist down to $f = 577.9$.

There are two main points to note concerning the intermediate-f branch of solutions and how its terminal point relates to the small-f branch of solutions. Firstly the two branches cross over in all the above examples, and so there is a value of f at which the most unstable mode will change from being one associated with the small-f branch to one associated with the intermediate-f branch. Secondly, we note that we can use these results to show when the two branches of solutions cease to overlap, and hence this whole asymptotic structure must cease to exist.

If we take the result (4.25c) for the critical value of H on the intermediate branch of solutions and find when it takes the corresponding value to that obtained in the non-rotating slot (which is correct to within 8% for the whole small-f branch) we find that the two branches will cross when

$$f = 3\sigma\left(\frac{\pi^2 R}{4\tau}\right)^{1/6}. \tag{4.28}$$

The terminations of the small- and intermediate-f branches are given by (4.14a) and (4.27) respectively. These are equal when

$$\frac{\tilde{f}}{f} = \frac{(1-\tau)^2 H^2}{R^2} = 0.2632. \tag{4.29}$$

Again using the critical values for the non-rotating case gives the minimum value for R for which the two-branches overlap as

$$R = 2\,307\,000\tau. \tag{4.30}$$

For the value $\tau = 1/80$ that we have been using, this gives $R = 28\,840$. This is more than the value of $R = 10^4$ for which we found that there were the separate branches of solutions, but it is clear from figure 5 that for this value of R the intermediate-f solutions did not really exist. However, this value does give the correct order of magnitude for the termination of the two-branch structure.

5. Primary balances for large R

Having found the various asymptotic behaviours in the previous section it is instructive to determine which terms in the governing equations give rise to the various asymptotic regimes, and so identify the balance of forces which have a role in the dynamics of double-diffusive instabilities in a rotating slot.

For the case of the small-f branch of solutions the primary simplification occurs in the difference in the vertical and horizontal length scales. The vertical scale is given by the Chen height, while the horizontal scale is given by the slot width. This leads to the simplification in the governing equations (2.1a–d) that the diffusive fluxes are primarily in the vertical direction and so we can use the approximation $\nabla^2 \approx \partial^2/\partial z^2$. Further simplification can also be made when f is small. With both v and l being of order f in magnitude one can simplify the problem further by ignoring the $O(f^2)$ terms which will result in the y-component of the momentum equation (2.1a) being the only one that has any terms that are not also present in the non-rotating case. This will then give an equation for finding v given the non-rotating solution and the along-wall component of the wavenumber, l. However to find the value of l corresponding to the most unstable mode one would also have to examine the $O(f^2)$ balances. This is not done here.

One important balance that can occur in a rotating system is a geostrophic balance between horizontal pressure gradients and the Coriolis forces. This occurs when the length scales of the motions exceed the internal Rossby radius of deformation (see, for example, Gill 1982). The Rossby radius in a uniformly stratified fluid is determined by the vertical length scale of a disturbance. In dimensional units the Rossby radius for a disturbance of height h is

$$L_h = Nh/f \tag{5.1}$$

where $N^2 = -g\,(\mathrm{d}\rho/\mathrm{d}z)\,/\rho_0$ is the Brunt–Väisälä or buoyancy frequency (Rayleigh 1883). Thus one of the important considerations in this problem is whether the Rossby radius for a given disturbance is of a similar size to the slot width. For disturbances that are limited to the Chen scale this radius is equal to the slot width when the rotation rate is given by

$$f^2 = \frac{g(\alpha\Delta T)^2}{-\beta\bar{S}_z}. \tag{5.2}$$

In non-dimensional terms appropriate for the small-f branch this is equivalent to

$$\tilde{f}^2 = \frac{\sigma\tau Q}{(1-\tau)^2}. \tag{5.3}$$

This is the order of magnitude at which the small-f branch of solutions terminates.

The simplifications involved in the intermediate branch of solutions concern the z-component of the momentum equation, (2.1a). If we replace it with the simple relationship

$$0 = g(\alpha T - \beta S) \tag{5.4}$$

while leaving all the other governing equations unchanged, then the characteristic equation that would be obtained is (4.26). Thus in this intermediate branch of solutions the leading approximation from the z–component of the momentum equation is that there is no density perturbation.

If one assumes that the vertical length scale is comparable to the width of the slot then the non-dimensional rotation rate at which the Rossby radius is the same as the

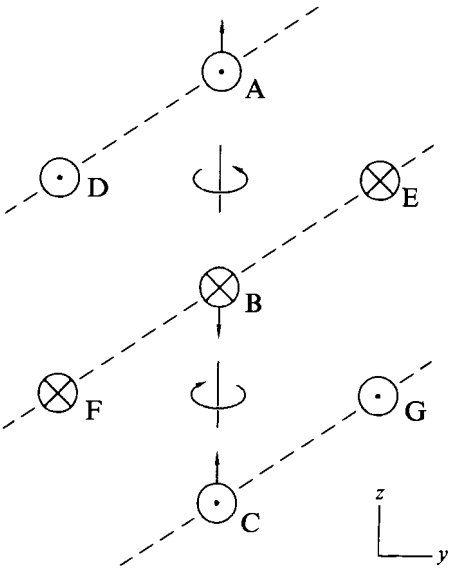

FIGURE 10. Diagram indicating the vorticity for the intermediate-f solutions. This is viewed from the hot wall. The $\otimes$ indicate regions where the fluid is going away from the hot wall, while the $\odot$ indicate regions where the fluid is coming towards the hot wall. See text for discussion.

width of the slot is given by

$$f^2 = \sigma R. \tag{5.5}$$

This corresponds to the transition from the intermediate- to the large-f branch of solutions and so for the intermediate-f branch of solutions there is no geostrophic balance. If one looks at the horizontal momentum equation we see that there is still a balance between the generation of vorticity due to vortex stretching and its dissipation due to viscosity.

As a parcel of fluid moves from the hot salty wall towards the cooler fresher wall it will lose its heat faster than it will lose its salinity. Thus it will become denser. As (5.4) requires that there are no density perturbations, it must sink to a region of denser fluid. Similarly, parcels of fluid moving towards the warmer saltier wall must rise. If one considers periodic convection cells up a wall (see figure 10) then in the region below an area where the fluid is moving towards the warmer saltier wall (A) and above a region where it is moving away from this wall (B) the fluid elements will be stretched in the vertical direction. Thus vertical vorticity with the same sense of rotation as the system as a whole is being generated in this region. For positive f this will lead to the fluid circulating in an anticlockwise direction when viewed from above. This will tend to make fluid on either side of this region of vortex stretching circulate in the directions shown in the figure at D and E. Similarly, if one considers the fluid below a region where the fluid is moving away from the saltier warmer wall (B) and above a region where it is moving towards the hotter wall (C) then vorticity of the opposite orientation is generated as shown. When these results are combined it shows that the slope of the rolls along the wall will be up in the positive y-direction for positive f as shown. This is the orientation that was shown in figure 6.

Consideration of this balance between the generation of vorticity by this means and by viscous dissipation shows why the intermediate-f branch of solutions terminates when it does for lower values of f. If a typical velocity in a convection cell is U,

then the rate of stretch per unit length in the vertical direction will scale as U/d for disturbances of the same vertical scale as the slot width. Thus the rate at which vorticity is added scales as fU/d. However, the typical vorticity will scale like U/d, and so the rate at which vorticity is lost is $\nu U/d^3$. For disturbances to continue to exist we must have the rate of generation of vorticity being greater than the rate it is dissipated, or

$$\frac{fU}{d} > \frac{\nu U}{d^3}, \tag{5.6}$$

or

$$f > \frac{\nu}{d^2}. \tag{5.7}$$

This is indeed the balance that was observed in the results of §4.3 where the non-dimensional value of f at which the intermediate branch of solutions ended was found to be proportional to the Prandtl number as (5.7) would imply.

We can also use a mechanistic argument to give the correct scaling for the critical temperature difference for this branch of solutions. If we consider a parcel of fluid that is displaced horizontally by a distance δx towards the hot wall it will find itself in a region where the average temperature is approximately $\delta x \overline{T}_x = \delta x \Delta T/d$ hotter than its original temperature. It will gain heat and so rise by a distance

$$\delta z \approx \delta x \alpha \Delta T/(-\beta \overline{S}_z d) \tag{5.8}$$

in order to be in fluid of its own density (because of the large difference in the diffusivities of heat and salt the diffusion of salt can effectively be neglected here). Conservation of angular momentum tells us that if a column of fluid is stretched or compressed along its axis of rotation then the ratio between its vorticity, ω, and its height, h, remains constant. If we assume a vertical periodicity of P, the change in the vorticity of the column below the fluid parcel will scale according to

$$f/P \approx (f + \delta\omega)/(P + \delta z), \tag{5.9}$$

giving

$$\delta\omega \approx f\delta z/P. \tag{5.10}$$

This will induce a typical horizontal velocity of order $u_0 \sim \delta\omega d$ in this region. Viscous dissipation of a parcel of fluid at this higher level will mean that any velocity will decay approximately as $\mathrm{d}u/\mathrm{d}t \sim -\nu u/d^2$ if the horizontal scale is smaller than the vertical scale, or $\mathrm{d}u/\mathrm{d}t \sim -\nu u/P^2$ if the vertical scale is the smaller. Integrating twice with respect to time gives a typical horizontal displacement of $\delta x' = u_0 d^2/\nu$, or $\delta x' = u_0 P^2/\nu$ if the vertical scale is smaller than d. Combining all these scales gives $\delta x' \sim f\delta z d^3/P\nu$ if $P > d$ and $\delta x' \sim f\delta z dP/\nu$ if $P < d$. Since the former is increased by reducing P and the latter by increasing it, it is clear that $\delta x'$ will be maximized when P and d are of similar size, giving

$$\delta x' \sim f d^2 \delta z/\nu. \tag{5.11}$$

This horizontal displacement will induce motions in the original layer by the same mechanism, and so for self-sustaining motions we would require that $\delta x'/\delta x > 1$. From the above argument we can find the scaling of this ratio,

$$\delta x'/\delta x \sim \alpha \Delta T f d/(-\beta \overline{S}_z \nu) = fH/\sigma R, \tag{5.12}$$

and so we would expect that for an instability to be self-sustaining the critical value

of H would scale as $\sigma R/f$. This is the scaling found in the previous intermediate-f branch analysis of § 4.3.

For the large-f branch of solutions the vertical component of the wavenumbers, m, becomes small as the rolls align themselves with their axes becoming more vertical. This leads to the exact opposite to the small-f branch of solutions in that in the diffusion terms the fluxes in the horizontal directions dominate, while those in the vertical direction can be ignored. Hence we can approximate $\nabla^2 \approx \partial^2/\partial x^2 + \partial^2/\partial y^2$. In the z-momentum equation the viscous term can again be ignored, but this time the vertical pressure gradient term must be retained, giving

$$0 = -\frac{1}{\rho_0}\frac{\partial p}{\partial z} + g(\alpha T - \beta S). \tag{5.13}$$

Thus the pressure is given to leading order by the hydrostatic approximation. This large-f branch of solutions differs from the intermediate-f solutions in that the Rossby radius for the convection cells is comparable to the slot width. In such circumstances the balance between the horizontal pressure gradients and the Coriolis force comes into play, leading to a more complex interaction than in the intermediate-f case.

6. Instabilities driven by varying horizontal gradients

In this section we derive the stability criteria for convection in the case where there are variable horizontal temperature and salinity gradients. Kerr (1989) showed that for large vertical salinity gradients it is possible to make a quasi-static assumption based on the observation that in the non-rotating case the instabilities grow on a time scale based on the thermal diffusion time over the Chen scale, while the background gradients evolve over a time scale based on the diffusion time over the horizontal scale of the thermal anomaly. From the discussion in the previous section it is clear that for both the intermediate- and large-f branches of solutions, horizontal diffusion plays an important role in the onset of convection, and so a quasi-static assumption which requires that horizontal diffusion is negligible will break down. For these reasons we will only derive the governing equation for strong stratification and low rotation rates.

For more general horizontal temperature gradients we can no longer assume that at marginal stability the growth rate λ is zero. Instead it will in general be imaginary. However, we can still assume for strong vertical salinity gradients that at leading order the background state has no horizontal density gradient, i.e. the horizontal temperature and salinity gradients are compensating. Making the same assumptions that were made for the small-f branch of solutions, the non-dimensional governing equations become

$$(\mathrm{i}\tilde{\omega} + \sigma\tilde{m}^2)u - \tilde{f}v = -p', \tag{6.1a}$$

$$(\mathrm{i}\tilde{\omega} + \sigma\tilde{m}^2)v + \tilde{f}u = -\mathrm{i}lp, \tag{6.1b}$$

$$0 = -\mathrm{i}\tilde{m}p + \frac{Q}{1-\tau}(T - S), \tag{6.1c}$$

$$(\mathrm{i}\tilde{\omega} + \tilde{m}^2)T + uF'(x) = 0, \tag{6.1d}$$

$$(\mathrm{i}\tilde{\omega} + \tau\tilde{m}^2)S + uF'(x) - (1-\tau)w = 0, \tag{6.1e}$$

$$u' + \mathrm{i}lv + \mathrm{i}\tilde{m}w = 0, \tag{6.1f}$$

where primes denote derivatives with respect to x. The imaginary growth rate, $\tilde{\omega}$, has a tilde to make it clear that this non-dimensional frequency is scaled according to the

time scale based on the Chen height and not the slot width. Note also that just as in the case of the small-f equations for large values of R, the viscous diffusion term, and also the time-derivative term can be neglected in the vertical momentum equation. Again the primary balance in this equation gives the hydrostatic approximation.

If we define $\Gamma(x)$ by

$$\left(\frac{\mathrm{d}^2}{\mathrm{d}x^2} - l^2\right)\Gamma(x) = w(x) \tag{6.2}$$

then (6.1a)–(6.1f) can be reduced to a second-order differential equation:

$$\begin{aligned} 0 = &\left(\frac{\mathrm{d}^2}{\mathrm{d}x^2} - l^2\right)\Gamma(x) + \frac{\tilde{m}^2 F'(x)}{\mathrm{i}\tilde{\omega} + \tilde{m}^2}\left(\mathrm{i}m\frac{\mathrm{d}}{\mathrm{d}x} - \frac{fl\tilde{m}}{\mathrm{i}\tilde{\omega} + \sigma\tilde{m}^2}\right)\Gamma(x) \\ &- \frac{\tilde{m}(\mathrm{i}\tilde{\omega} + \tau\tilde{m}^2)(\mathrm{i}\tilde{\omega} + \sigma\tilde{m}^2)\Gamma(x)}{\sigma\tau Q} - \frac{f^2\tilde{m}^2(\mathrm{i}\tilde{\omega} + \tau\tilde{m}^2)\Gamma(x)}{\sigma\tau Q(\mathrm{i}\tilde{\omega} + \sigma\tilde{m}^2)}. \end{aligned} \tag{6.3}$$

If $f = l = 0$ this equation simplifies to the adjoint of equation (3.20) of Kerr (1989). At the wall, the boundary condition that $\Gamma(x)$ must satisfy corresponds to no fluid flux through the wall ($u = 0$), and is

$$\left(-\mathrm{i}\tilde{m}\frac{\mathrm{d}}{\mathrm{d}x} + \frac{\tilde{f}l\tilde{m}}{\mathrm{i}\tilde{\omega} + \sigma\tilde{m}^2}\right)\Gamma(x) = 0. \tag{6.4}$$

If the gradients are located in an unbounded fluid with the horizontal gradients decaying in the far field then the appropriate boundary condition in this far field is that $\Gamma \to 0$.

For a constant gradient this problem reduces to that considered earlier in the small-f asymptotics for large R.

This eigenvalue problem can be solved numerically using standard techniques for given l and $\tilde{m}$ to give the corresponding Q and $\tilde{\omega}$. As before we can then minimize Q with respect to variations in l and $\tilde{m}$ to find the marginally stable mode. The results of such a calculation are shown in figure 11, showing Q, l, $\tilde{m}$ and $\tilde{\omega}$ as functions of $\tilde{f}$ that were calculated for an error function temperature profile $F(x) = \mathrm{erfc}(x/2)$. The results here are qualitatively similar to those obtained for a slot in the small-f regime. The differences are that there is now a drift of the instabilities down the wall implied by $\tilde{\omega} > 0$, and l is now positive since the horizontal temperature gradient at the wall is negative instead of being positive as was assumed before. The critical value of Q decreases as $\tilde{f}$ increases, and then the branch of marginally stable solutions vanishes at a critical value of f.

As with the case of a laterally heated slot, the existence of all of these solutions is not necessarily significant since the solutions are local. For larger values of $\tilde{f}$ it would be expected that there are other modes of instability corresponding to the intermediate- and large-f limits found in the vertical slot that would be more unstable. The above analysis relies on the difference between the time scale for the growth rate of the instabilities and the time scale for the evolution of the background gradients. The former is based on the short Chen length scale, while the latter is based on the longer slot width. The secondary branch of solutions for the slot, with its intermediate- and large-f regimes, has a time scale for the evolution of the instabilities that scales with the slot width. Thus both the instabilities and the background gradients will evolve on a similar time scale and so their investigation will not be accessible using a quasi-static approximation.

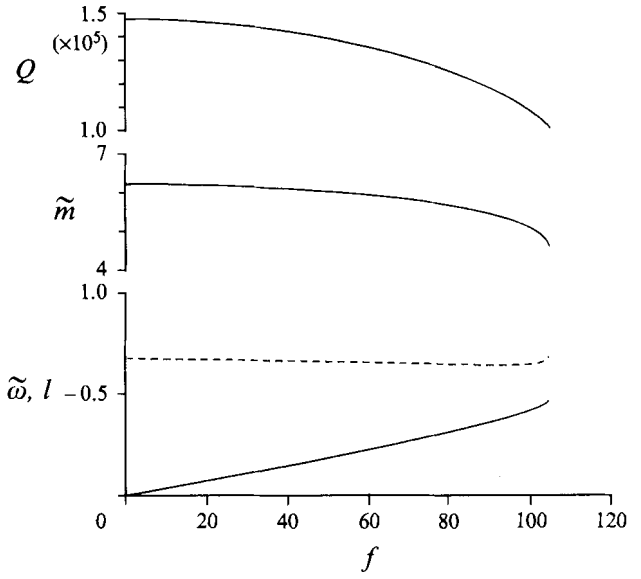

FIGURE 11. Values of Q, $\tilde{m}$, $\tilde{\omega}$ (- - - - -) and l for marginal stability for a rotating salinity gradient heated from an isolated vertical wall assuming an error function temperature profile.

7. Conclusions

We have investigated the marginal stability of a rotating fluid with a vertical salinity gradient in a laterally heated slot. Using simplified boundary conditions, we have shown that in the limit of strong stratification there are three different regimes for the onset of instability. The first of these, referred to here as the small-f regime, is essentially the same mode of instability that has been identified before in a non-rotating frame of reference, but with modification due to the effects of rotation. Rotation has a destabilizing effect on these instabilities, although the effect is not strong. The rotation also caused the almost horizontal flat convection cells to develop a slope in the horizontal direction parallel to the walls. This slope mimics that predicted for the case of double-diffusive interleaving in an unbounded fluid with constant horizontal and vertical temperature and salinity gradients. The vertical scale of this mode of instability is governed by the Chen scale. This branch of instabilities terminates when the Rossby radius based on this vertical scale becomes comparable to the width of the slot.

The first mode of instability is not always the most unstable mode, the other two modes may be more unstable. These other modes together form a continuous branch. The vertical scale of this branch is not limited by the Chen scale and the horizontal component of the wavenumber parallel to the vertical walls is almost exactly $-\pi/2^{1/2}$ for all values of f where these modes exist. The first of these two modes, referred to here as the intermediate-f branch of solutions, starts when the diffusion time of viscosity across the slot is comparable to the rotation rate. This convection mode is characterized by, to leading order, order-one slopes of the convection cells along the slot and no density perturbations. The motion of fluid elements is confined to almost horizontal planes which gently slope across the slot. The vertical motions in this plane lead to vortex stretching, which generates the vorticity required to drive the motions. As the rotation rate becomes stronger the Coriolis forces become more important, and when the Rossby radius based on a vertical scale comparable to the slot width becomes of a similar magnitude to the slot width itself the dynamics undergo a

further change. At this point horizontal density gradients can be supported, and the circulatory motions can be maintained with geostrophic balances. As the rotation rate increases the convection cells become more vertical, as would be expected from the Taylor–Proudman theorem.

The transition from the intermediate- to the large-f branch of instabilities occurs when the Rossby radius based on a vertical scale comparable to the slot width is of the same size as the slot width, while the small-f branch of solutions always terminates when the Rossby radius based on the Chen length scale is comparable to the slot width. As the Chen scale is assumed here to be less than the slot width this means that the small-f branch of solutions will always terminate before the large-f branch of solutions begins. Thus, as the rotation rate increases, the transition from the small-f branch will always be to the intermediate-f branch. So the form of the most unstable mode will change sharply from thin almost horizontal convection cells to cells with order-one aspect ratios and order-one slope parallel to the walls. The value of f at which this transition occurs is proportional to $(R/\tau)^{1/6}$.

The work presented here is related to the results of Yoshida *et al.* (1989) in their investigation of the influence of rotation on intrusive instabilities in a finite front when the salt and heat fluxes are dominated by the presence of salt fingers. With their model of the fluxes the front is always unstable, and so they looked at the fastest growing modes of instability. They too noted an abrupt jump in the vertical periodicity of the fastest growing mode as the rotation rate increases, corresponding to the transition between the small-f and intermediate-f branches of solutions found here. Because their flux model only accounts for fluxes in the vertical direction, and not the horizontal direction, there is no constraint on the horizontal scales due to increasing dissipation on smaller scales. This results in their model allowing the horizontal wavenumber, l, to increase without limit as f increases. Given the importance of horizontal diffusion in the intermediate-f and large-f branches here this may well indicate a limitation in the applicability of their model for larger values of f. However, the initial effects of rotation and the termination of the modes corresponding to the small-f branch of solutions found here would be well modelled in oceanographic situations where their flux laws are appropriate.

The direct application of these results to the experiments of Chereskin & Linden (1986) has to be done with caution for several reasons. Their experiment was in a different geometry, a heated circular cylinder in a large tank. Thus the analysis of §6 that can be applied to a semi-infinite body of fluid would be more appropriate. But the analysis in this geometry cannot be applied to the intermediate- and large-f branches of solutions as the quasi-static approximation cannot be applied. Also the system is not free to select any value of the horizontal wavenumber l, but only those that are compatible with a periodicity of the circumference of the cylinder. Thus the initial effect of the rotation would be, as the analysis of Chereskin & Linden suggests, to stabilize the fluid. In addition their observations are of finite-amplitude instabilities and not the infinitesimal instabilities considered here. It is known (Hart 1973; Kerr 1990) that in the non-rotating case such instabilities are likely to be subcritical, and so the observed instabilities may not closely resemble the prediction of the linear analysis. In addition their experiments were relatively rapidly heated, and so at the initial onset of instability the growth rate of the background horizontal temperature and salinity gradients will be comparable to the growth rate of any instabilities and so any prediction based on the assumption of steady background gradients must be made with caution. With these reservations in mind we should only look for qualitative agreement between the theory presented here and their experiments.

In the experiments of Chereskin & Linden the values of the vertical Rayleigh numbers using their definition varied from 4×10^4 to 2.37×10^7. Their definition differed in using the vertical Chen scale and not the horizontal extent of the thermal gradients used here. Since the horizontal extent of the intrusions tends to be larger than the vertical extent this would tend to imply that the vertical Rayleigh number of the experiments according to our definition would be appreciably greater than their values, and as such we are clearly in the large-R regime that we have considered. If we estimate the dimensional value of the rotation rate at which the transition from the small-f branch to the intermediate-f branch occurs from (4.28) we find that it occurs at around $0.3\,\mathrm{s}^{-1}$. Thus their rotating experiments should be in the regime where the instabilities are strongly affected by rotation. One of the predictions of the linear analysis is that the instabilities should have a large slope in the horizontal direction along the wall. In their experiments they noted that "dye observations indicate the layers spiral rather than merely slant downwards". They also noted that for larger rotation rates the vertical scale of the intrusions increased as the rotation rate increased. In some of their experiments the rotation rate did exceed the buoyancy frequency, but never by a factor of $(\sigma/\tau)^{1/2}$. So although the transition point to the large-f regime was never reached some of their experiments did get close enough for the initial trends to be observed, in particular the increase in the vertical length scale of the instabilities.

The investigation of the influence of rotation about a vertical axis on the double-diffusive instabilities in a vertical slot has shown how the effect of the rotation can become dominant even before the rotation may be anticipated to play an important role on the basis of arguments concerning the importance of the Rossby radius. This influence of the rotation on the interleaving instabilities will be important in many situations not readily amenable to a linear stability analysis based on the assumption of a steady background state, such as interleaving instabilities at fronts or at single side boundaries. Any analysis of such configurations would have to take into account the temporal evolution of the background temperature and salinity gradients.

REFERENCES

CHEN, C. F., BRIGGS, R. A. & WIRTZ, D. G. 1971 Stability of thermal convection in a salinity gradient due to lateral heating. *Intl J. Heat Mass Transfer* **14**, 57–65.

CHEN, C. F. & SANDFORD, R. D. 1977 Stability of time-dependent double-diffusive convection in an inclined slot. *J. Fluid Mech.* **83**, 83–95.

CHEN, C. F. & SKOK, M. W. 1974 Cellular convection in a salinity gradient along a heated inclined wall. *Intl J. Heat Mass Transfer* **17**, 51–60.

CHERESKIN, T. K. & LINDEN, P. F. 1986 The effect of rotation on intrusions produced by heating a salinity gradient. *Deep-Sea Res.* **33**, 305–322.

GILL, A. E. 1982 *Atmosphere-Ocean Dynamics*. Academic Press.

HART, J. E. 1971 On sideways diffusive instability. *J. Fluid Mech.* **49**, 279–288.

HART, J. E. 1973 Finite amplitude sideways diffusive convection. *J. Fluid Mech.* **59**, 47–64.

HOLYER, J. Y. 1983 Double-diffusive interleaving due to horizontal gradients. *J. Fluid Mech.* **137**, 347–362.

HOLYER, J. Y., JONES, T. J., PRIESTLY, M. G. & WILLIAMS, N. C. 1987 The effect of vertical temperature and salinity gradients on double-diffusive interleaving. *Deep-Sea Res.* **34**, 517–530.

HUPPERT, H. E. & JOSBERGER, E. G. 1980 The melting of ice in cold stratified water. *J. Phys. Oceanogr.* **10**, 953–960.

HUPPERT, H. E. & TURNER, J. S. 1980 Ice blocks melting into a salinity gradient. *J. Fluid Mech.* **100**, 367–384.

KERR, O. S. 1989 Heating a salinity gradient from a vertical sidewall: linear theory. *J. Fluid Mech.* **207**, 323–352.

KERR, O. S. 1990 Heating a salinity gradient from a vertical sidewall: nonlinear theory. *J. Fluid Mech.* **217**, 529–546.

KERR, O. S. & HOLYER, J.Y. 1986 The effect of rotation on double-diffusive interleaving. *J. Fluid Mech.* **162**, 23–33.

LINDEN, P. F. & WEBER, J. E. 1977 The formation of layers in a double-diffusive system with a sloping boundary. *J. Fluid Mech.* **81**, 757–773.

MCDOUGALL, T. J. 1985 Double-diffusive interleaving I. Linear stability analysis. *J. Phys. Oceanogr.* **15**, 1532–1541.

NIINO, H. 1986 A linear theory of double-diffusive horizontal intrusions in a temperature-salinity front. *J. Fluid Mech.* **171**, 71–100.

PALIWAL, R. C. & CHEN, C. F. 1980 Double-diffusive instability in an inclined fluid layer. Part 2. Stability analysis. *J. Fluid Mech.* **98**, 769–785.

PEARLSTEIN, A. J. 1981 Effect of rotation on the stability of a doubly diffusive fluid layer. *J. Fluid Mech.* **103**, 389–412.

POSMENTIER, E. S. & HIBBARD, C. B. 1982 The role of tilt in double-diffusive interleaving. *J. Geophys. Res.* **87**, 518–524.

RAYLEIGH, LORD 1883 Investigation of the character of the equilibrium of an incompressible heavy fluid of variable density. *Proc. Lond. Math. Soc.* **14**, 170–177.

RUDDICK, B. R. 1992 Intrusive mixing in a Mediterranean salt lens – Intrusion slopes and dynamical mechanisms. *J. Phys. Oceanogr.* **22**, 1274–1285.

RUDDICK, B. R. & TURNER, J. S. 1979 The vertical length scale of double-diffusive intrusions. *Deep-Sea Res.* **26**, 903–913.

SCHLADOW, S. G., THOMAS, E. & KOSEFF, J. R. 1992 The dynamics of intrusions into a thermohaline stratification. *J. Fluid Mech.* **236**, 127–165.

STERN, M. E. 1967 Lateral mixing of water masses. *Deep-Sea Res.* **14**, 747–753.

TANNY, J. & TSINOBER, A. B. 1988 The dynamics and structure of double-diffusive layers in sidewall-heating experiments. *J. Fluid Mech.* **196**, 135–156.

TANNY, J. & TSINOBER, A. B. 1989 On the behaviour of a system of double diffusive layers during its evolution. *Phys. Fluids* A **1**, 606–609.

THANGAM, S., ZEBIB, A. & CHEN, C. F. 1981 Transition from shear to sideways diffusive instability in a vertical slot. *J. Fluid Mech.* **112**, 151–160.

THORPE, S. A., HUTT, P. K. & SOULSBY, R. 1969 The effects of horizontal gradients on thermohaline convection. *J. Fluid Mech.* **38**, 375–400.

TOOLE, J. M. & GEORGI, D. T. 1981 On the dynamics and effects of double-diffusively driven intrusions. *Prog. Oceanogr.* **10**, 123–145.

TSITVERBLIT, N. & KIT, E. 1993 The multiplicity of steady flows in confined double-diffusive convection with lateral heating. *Phys. Fluids* A **5**, 1062-1064.

WALSH, D. & RUDDICK, B. R. 1995 Double-diffusive interleaving: the influence of non-constant diffusivities. *J. Phys. Oceanogr.* **25**, 348–358.

WORTHEM, S., MOLLO-CHRISTENSEN, E. & OSTAPOFF, F. 1983 Effects of rotation and shear on doubly diffusive instability. *J. Fluid Mech.* **133**, 297–319.

YOSHIDA, J., NAGASHIMA, H. & NIINO, H. 1989 The behaviour of double-diffusive intrusions in a rotating system. *J. Geophys. Res.* **94**, 4293–4937.